OCEANS 2022, Hampton Roads, October 2022
Pages 1-9
https://doi.org/10.1109/OCEANS47191.2022.9977221
https://archimer.ifremer.fr/doc/00813/92492/

In situ glider and remote-sensing satellite data synergy for the estimation of the PAR diffuse attenuation coefficient

De Nodrest Emma [1], Homrani Sabrina [2], Jourdin Frederic [3], Viellefon Priscille [4], Vient Jean-Marie [5], Durrieu De Madron Xavier Durrieu [6], Pasqueron De Fommervault Orens [7], Bourrin Francois [8]

[1] University of Bordeaux and CNRS,EPOC Laboratory,Bordeaux,France
[2] SEDIM Laboratory Shom,Brest,France
[3] University of Brest and CNRS,Geo-Ocean Laboratory,Plouzané,France
[4] UniLaSalle,Geology Department,Beauvais,France
[5] Lab-STICC Laboratory IMT-Atlantique,Plouzané,France
[6] CEFREM Laboratory CNRS,Perpignan,France
[7] ALSEAMAR ALCEN,Rousset,France
[8] UPVD University,CEFREM Laboratory,Perpignan,France

emma.denodrest@outlook.com ; sabrina.homrani@shom.fr ; fjourdin@univ-brest.fr ; priscille.viellefon@etu.unilasalle.fr ; jean-marie.vient@univ-brest.fr ; demadron@univ-perp.fr ; odefommervault@alseamar-alcen.com ; fbourrin@univ-perp.fr

Abstract :

Estimating the diffuse attenuation coefficient of the Photosynthetically Available Radiation (KPAR) allows to monitor primary production, dissolved organic matters, coastal suspended sediments and water transparency. The latter aim, especially for military purposes, may be efficiently achieved with the use of underwater gliders. The present study aims at estimating the KPAR in the the Bay of Biscay (North-East Atlantic), during a sea campaign which took place in February 2021, in fairly transparent waters mainly containing non-living suspended material. The sea survey involved a SEAEXPLORER glider equiped with an ocean color radiometer. The glider measurements were in agreement with those from shipboard CTD-PAR casts (with a mean relative difference of about 11%). VIIRS L2 and MODIS L4 satellite products were validated with the glider data. Accordingly, a bias correction has been proposed for the ocean color satellite KPAR algorithm.

Keywords : KPAR, glider, bathysonde, satellite products, optical properties, ocean color algorithms

A

I. Introduction

Coastal areas are key in the transport and storage of suspended matters from watersheds to the ocean, it is therefore important to quantify the associated concentrations and fluxes. These suspended matters include sediment particles, living algae, organic matters, nutrients and contaminants, which influence and control the functioning of coastal ecosystems [1].

Routine measurements of concentrations and fluxes are most commonly acquired by fixed moorings, such as buoys or benthic landers. In addition, the concentration of surface suspended matters and dissolved materials can be estimated at large spatial scales by the deployment of space-based or airborne sensors measuring their optical characteristic signatures. This is commonly referred to as "water color". However satellite imagery is limited: few images are usable during intense meteorological events, like storms, due to a significant presence of clouds, while in addition fluxes are most significant during these episodes. Moreover, the satellite's revisiting period over a same area is of the order of one image per day. On the contrary, underwater gliders benefit from a higher rate of acquisition and, as autonomous platforms, can observe a dedicated oceanic area during storms.

The MELANGE[1] project aims at automating the acquisition and processing of data acquired by the SEAEXPLORER gliders (ALSEAMAR-ALCEN company, France), so as to measure simultaneously and in quasi real-time both the current and turbidity; and thus to obtain the particulate fluxes [1].

In this article, the ocean color parameter chosen to perform an initial validation on the use of the SEAEXPLORER glider is the diffuse attenuation coefficient of the Photosynthetically Available Radiation (K_{PAR}). Measuring K_{PAR} values makes possible the monitoring of primary production, fluxes of suspended sediments and dissolved organic matter from the

[1]Mesure en tEmps-réel des fLux sédimentAires en zoNe côtière à l'aide de Gliders

coast to the open sea, or simply to evaluate the transparency of the water for military purposes.

Firstly, the present study aims at comparing the K_{PAR} data issued from the glider with those from a bio-optical CTD probe deployed simultaneously from the research vessel "Thalassa", which was sailing nearby (within less than 10 NM from the glider). Subsequently, all measurements from the glider are compared to the optical parameters obtained from the satellite water color imagery. Then, some "matchups" (coincidental comparisons in space and time between satellite and glider) are found. Consequently the quality of the satellite products is discussed in relation to in situ data, whose spatial and temporal scales of observation are finer than those of the dedicated satellites.

II. Materials and Methods

A. Field validation campaign

A SEAEXPLORER glider was deployed during a field campaign that took place on the continental shelf north of the Bay of Biscay. The campaign took place in winter conditions, from February 14, 2021, at 07:30 (UTC) to February 18, 2021, at 13:00 (UTC). The study area was located 40 NM from the French coast, and covered a rectangular area of 12 NM by 13 NM (Fig.1), with an average ocean depth of 115 ± 4 m. This area is located around a SHOM key point: "La Grande Vasière" (mid-shelf mud belt). It has been monitored regularly since 2007 by the SHOM because it is a well-known bottom trawling area. Trawlers disturb the biotope at the water-sediment interface and resuspend sediments. This resuspension causes an anthropogenic increase in bottom turbidity, leading to a decrease in light conditions for benthic organisms [2].

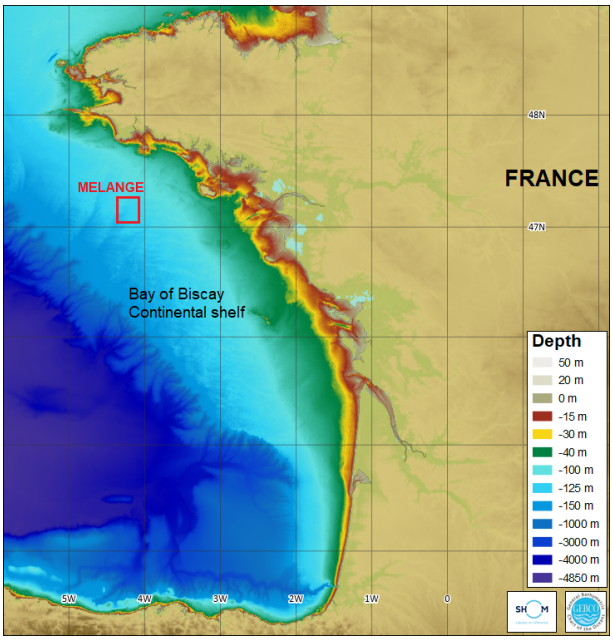

Fig. 1. MELANGE campaign area location, with the bathymetry of the Bay of Biscay (SHOM, 2015).

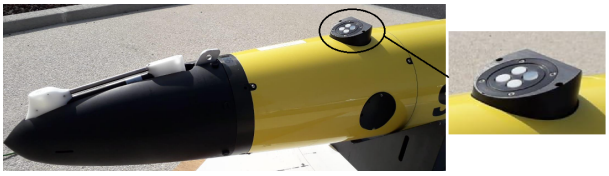

Fig. 2. Sea-Bird PAR sensor model OCR-504, onboard ALSEAMAR glider model SEAEXPLORER. The sensor is attached to the glider in such a way that it is optimally oriented during glider's ascents.

B. Glider and CTD probe deployment strategy

Ocean gliders are a complementary mean to perform underwater surveys and oceanographic data collection missions, compared to ships or moorings. Sailing autonomously in the water for weeks or even months, and traveling hundreds of miles even in stormy weather, gliders collect various data (physical, chemical, biological, acoustic, etc.) along the water column [3]. Various sensors and probes can be assigned to them. These data are then sent via satellite telemetry to a ground station [3]. Gliders move through the water column by changing their buoyancy through a ballast system, diving along with an oblique angle and describing up-and-down trajectories called "yos", i.e. by repeating a basic yo pattern, they move along a saw-tooth trajectory.

During the campaign, the glider was equipped with a GPCTD (Glider-Pumped Conductivity, Pressure, Temperature, from Seabird) probe; an AD2CP (glider dedicated Acoustic Doppler Current Profiler, from Nortek) for acoustic backscatter and current measurements; an irradiance sensor (Seabird OCR-504) at three wavelengths (380, 490 and 532 nm) plus a fourth channel reserved for integrated measurement over the full visible range, the PAR (Fig.2); a triplet (Wetlabs FLBBCD) for measuring optical backscatter at 700 nm (called hereafter turbidity), fluorescence of chlorophyll-a (Chla), and CDOM (Coloured Dissolved Organic Matter); and a dissolved oxygen sensor.

Glider PAR measurements were acquired by its Seabird OCR-504 sensor, from the ocean surface to the seafloor ($\approx$ 120 meters). Data from night, sunset and sunrise-times were not taken into account for the study, as the optimal sun height above the horizon for the acquisition of an apparent optical property (AOP) like K_{PAR} should be higher than 20° [4]. Moreover, only data acquired during glider ascents were processed. Indeed, the glider ascends and descends in the water column with a given pitch angle, and the Seabird OCR-504 sensor, attached to the glider, is tilted at an angle so as to capture all the light energy from the upper half-plane during ascents only. On the other hand, during the descent, the sensor is thus oriented at a very oblique angle, which biases the irradiance and associated PAR measurements (Fig.2). Raw data were acquired at the rate of 1 Hz. These data were post-processed at the ALSEAMAR company. This process mainly consists in a moving average so as to get final data every 5 seconds. This increases the signal-to-noise ratio while keeping a suitable spatiotemporal resolution for our purpose. Indeed,

knowing that the glider ascends with a mean vertical speed of around 0.2 m/s, we then get a PAR value for every meter of depth, which is enough to profile the decrease of PAR values with depth in the fairly clear waters of our area of study (a few Secchi disk observations gave values around 7 m). The K_{PAR} was computed as the slope coefficient deduced from a linear regression applied from the surface to the maximum measured depth, according to the following formula:

$$\text{-ln}(PAR) = K_{\text{PAR}} \times z \tag{1}$$

Where -ln(PAR) is the Napierian logarithm of PAR (or C_{PAR} for the shipborne CTD probe data) and z is the depth.
The raw data showed that, from a given irradiance level, the linear decrease in irradiance values as a function of depth was no longer respected, and data formed a plateau, at a depth of about 50 meters; it gave the minimum detection threshold of the sensor. Beyond this threshold, the data were not taken into account. To validate measurements acquired by the glider, a CTD probe equipped with bio-optical sensors was deployed from the R/V "Thalassa", during the first and last day of the cruise. Equipped bio-optical sensors were an optical backscatter sensor at 700 nm for turbidity, Chla and CDOM fluorometers, an optical transmissometer, a laser particle size analyzer, and a PAR quantameter (LI-COR Biospherical QSP2300). On the ship, a probe equipped with a S_{PAR} (surface PAR) sensor was fixed above the upper deck. This is a LI-COR Biospherical QSR2200 Surface PAR sensor, which has a uniform sensitivity over the entire PAR waveband for accurate outdoor measurements. This sensor is used in this study as a reference and allows to correct PAR data from variations of cloudiness, and thus to obtain a corrected PAR, called C_{PAR}, such as:

$$\frac{PAR}{S_{\text{PAR}}} = \frac{PAR_Z}{PAR_0} = C_{\text{PAR}} \tag{2}$$

Where PAR_Z is the PAR at a depth z and PAR_0 is the PAR at 0 meter of depth (ocean surface).
Using a S_{PAR} probe could cause an additional problem: the shadow of the mast. Thankfully, S_{PAR} profiles did not apparently show any shading from the ship's mast during the field campaign. Furthermore, S_{PAR} profiles did not show significant variations due to cloud cover dynamics during the CTD casts acquisition (data not shown). This implies that there were probably no problems related to cloud cover variations during glider ascents.
As for the glider, a linear regression of C_{PAR} data in relationship to depth was plotted. Moreover, C_{PAR} data acquired when the irradiance was low or non-existent were not taken into account. Data beyond the 50 meters depth threshold were discarded for the same reasons as mentioned above.
A relative difference was calculated to get an idea of the variability between the two data sets, using the glider point closest to the shipborne CTD cast point, for the same day of acquisition (in this case, for February 14th and 18th). The relative difference is computed according to:

$$\delta\alpha r = \left| \frac{K\text{par}_{\text{glider}} - K\text{par}_{\text{bathysonde}}}{K\text{par}_{\text{bathysonde}}} \times 100 \right| \tag{3}$$

TABLE I
SATELLITE DATA CONSIDERED IN THE STUDY. THE RESOLUTION CHOSEN IS THE HIGHEST AND MOST ACCURATE AVAILABLE IN EACH DATASET. OUTPUTS OF THE [10] ALGORITHM WERE MADE PUBLICLY AVAILABLE BY F. GOHIN ON HIS OWN IFREMER FTP. THE DINEOF INTERPOLATION CORRESPONDS TO DATA INTERPOLATING EMPIRICAL ORTHOGONAL FUNCTIONS ([6];[7]; [19];[20]))

Product	Sensor	Satellite	Algorithm	Interpolation
L2 [21]	MODIS	AQUA	Empirical	NA
L2 [22]	VIIRS	NPP-SUOMI	[10]	NA
L3 daily [23]	OLCI	S3A/3B	Semi-analytical [24]	NA
L4 [25]	MODIS	AQUA	Empirical	OI
L4 [8]	MODIS	AQUA	[10]	DINEOF

C. Satellite products

Satellite products of the ocean color used in this study are presented in Table I. They include Level-2 (L2) and Level-4 (L4) data. L2 products correspond to cloudy images of ocean surface bio-geophysical parameters deduced from optical algorithms (either empirical or semi-analytical). L4 products are cloud-free images, where values in cloudy areas are completed using interpolation methods. Here two interpolation methods were considered: Optimal Interpolation (OI) and Data Interpolating Empirical Orthogonal Functions (DINEOF). The OI, or kriging method [5], is a geostatistical method of linear estimation of data and guarantees a minimum variance. It performs a spatiotemporal interpolation conditioned by the spatiotemporal covariance of the data. For more information on the OI used here, refer e.g. to the study of [6]. The DINEOF interpolation method reconstructs missing information from an incomplete data set following a principal component analysis, using Empirical Orthogonal Functions (EOF), applied to a first guess of interpolated values. This is an iterative method, which yields the temporal and spatial shape of data (patterns) in an optimal frame. In summary, EOFs allow for the synthesis of information to facilitate analysis [7]. The DINEOF interpolation used here has been performed by our team, and comes from the study of [8], where the interpolation was applied on L2 MODIS products from 2003 to 2011 (for learning) and applied to the year 2021 (for restitution).

For each available matchup, i.e. when an in situ data is located exactly in a satellite image pixel, the relative error ($\delta\alpha$r) between both satellite and in situ data, and the time difference (ΔH) between the satellite and glider acquisition's timetables were computed. A window of $\pm$ 3 hours was assigned around the time of satellite passage over the MELANGE zone, to avoid large temporal gaps [9].

D. Algorithm of Gohin et al. (2005) [10]

The study by [10] focused on the analysis of satellite-derived parameters for biological modeling in coastal waters of the Bay of Biscay. One particular aim was to estimate the relationship between the diffuse light attenuation coefficient and concentrations of Chla and Non Algal Particles (or NAP). They used the SeaWiFS satellite product database, using a look-up table described in [11], from 1998 to 2003. It includes surface measurements of NAP, Chla concentrations, and irradiance profiles, from which the K_{PAR} is derived. In this study, statistical properties were used, based on in situ and colocated satellite-derived data, in order to express K_{PAR} by a power law combination of Chla and NAP concentrations. Variograms between satellite data and in situ Chla, NAP concentrations and K_{PAR} data were studied. The variograms showed quite a strong correlation of K_{PAR} with NAP but a lower correlation with chla, due to inter-relationship between all these three parameters. Results allowed to propose a relationship, based on NAP and Chla, to estimate K_{PAR} on the Bay of Biscay continental shelf. However, due to a low number of K_{PAR} data, the K_{PAR} variogram appeared to have a poor structure, and this led to quite large errors in this following correlation power law:

$$K_{\text{PAR}} = 0.1 + 0.0625[NAP] + 0.05[Chla]^{0.80} \quad (4)$$

This first type of equation originates from the study of [12] for the determination of inherent optical properties based on underwater illumination measurements in the Irish Sea.
However, after a change in the database by Francis Gohin, [13] showed that using a coefficient of 0.06 in the first term of the equation was more appropriate than the coefficient of 0.1, especially for clear waters with relatively low K_{PAR} coefficients ($\leq 0.1\ m^{-1}$). The equation (4) thus became :

$$K_{\text{PAR}} = 0.06 + 0.05[NAP] + 0.05[Chla]^{0.75} \quad (5)$$

In the context of the MELANGE project, a first comparison of in situ glider data and satellite K_{PAR} data (derived from equation (5)) was carried out and showed that the second version of the [10] algorithm was not adapted to the water masses studied. Indeed, the K_{PAR} study showed significant disagreements between data from field observations and data derived from satellite measurements. Calculated relative errors were 93% between in situ K_{PAR} data and L2 product data and 86% with L4 product data using optimal interpolation.
Research has been carried out in order to bring a new correction to the algorithm of [10], in order to adapt the K_{PAR} formula to studied waters, because coefficients lower than 0.06 m^{-1} could be observed during the campaign. The work of [10] is based on water types relatively concentrated in suspended matter and Chla, resulting in a high diffuse light attenuation coefficient. However, the type of water studied during the MELANGE campaign presents quite a low turbidity which induces lower attenuation coefficients. Our bibliographic research has therefore been focused on optical studies dedicated to clear waters. In particular, [14] reported

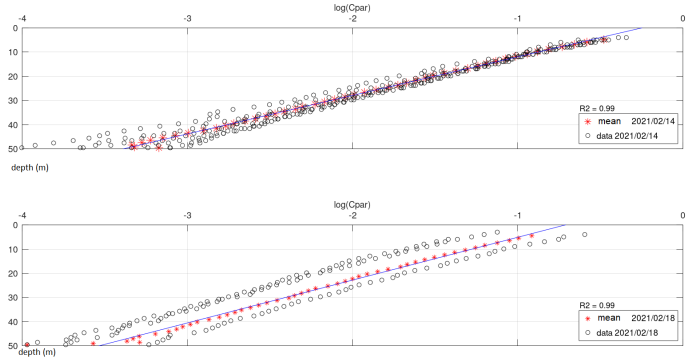

Fig. 3. Log(C_{PAR}) data from the CTD probe as a function of depth for the 2 days of acquisition: February 14 (up) and 18 (down), 2021. In order to adjust the graphical representation, the blue line corresponds to an example of linear regression, applied on the daily mean, which is represented by the red dotted line. The black dotted lines correspond to the different profiles during the day.

in 2016 on the study of the ultraviolet absorption spectrum (between 250 and 550 nm) of pure water and found an absorption coefficient of pure water at 490 nm of 0.0146 m^{-1} with a standard error value of 0.00054. Based on this study, assuming a negligible backscatter diffusion value for pure water [15], and following Gordon's approximation of the diffuse attenuation [16], the [10] formula has been corrected using a new intercept:

$$K_{\text{PAR}} = 0.015 + 0.05[NAP] + 0.05[Chla]^{0.75} \quad (6)$$

Also, for information, studies from Morel and Maritorena [17] found a value of about 0.017 for the $K_{\text{d}}490$ of pure water, and the minimum value of K_{PAR} measured by Biogeochemical-Argo (BGC-Argo) floats in [18] (see their Table 1) appeared to be 0.025.
In the following, the algorithm (6) will be called the corrected algorithm.

III. Results and Discussion

A. Glider versus CTD probe

The logarithm of C_{PAR} values acquired by the CTD probe was plotted as a function of depth. All profiles obtained are presented in Fig.3 superimposed with the daily average profile in red and its linear regression blue line for clarity. In the same way, the logarithm of PAR values acquired by the glider was plotted and displayed in Fig.4. At first sight, slopes of the main profiles obtained with either the glider or the CTD probe appear to follow similar trends. Moreover results showed a completely linear decay of the logarithm of C_{PAR}, with a low variability in the data during the campaign. In other words, no variation of K_{PAR} with depth was observed, up to the minimum irradiance threshold. Results obtained with the glider are similar: a linear decrease of the logarithm of PAR with depth. After performing linear regressions, the CTD probe profiles gave an average K_{PAR} of 0.14 ± 0.02 m^{-1}, and the glider 0.12 ± 0.02 m^{-1} (for the whole campaign). The resulting relative difference (computed as explained in the end of Section II-B) was nearly 13% for February 14th

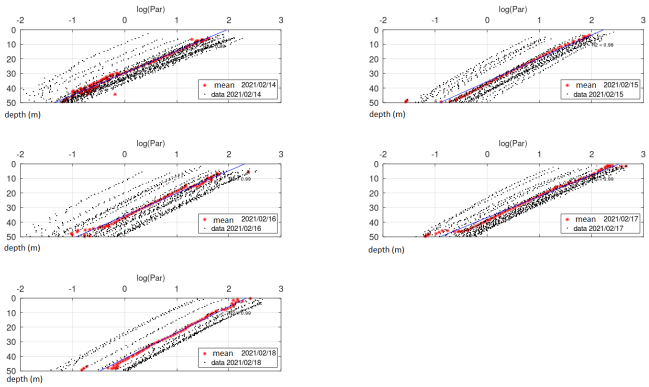

Fig. 4. Log(PAR) data of the glider as a function of depth over the 5 days of the MELANGE campaign (reading order). In order to adjust the graphical representation, the blue line corresponds to an example of linear regression, applied on the daily mean, which is represented by the red dotted line. The black dotted lines correspond to the different profiles during the day.

and 8% for February 18th, giving an average difference of 11%, and an average correlation coefficient equal to 0.63. The two datasets are then in excellent agreement with a low relative error, despite a correlation coefficient of 0.63. This low correlation may explain additional spatiotemporal variability of the K_{PAR} data in the considered study area.

Results obtained allow discussing about the type of water mass encountered. First of all, the water masses present vertically homogeneous profiles (as recorded by the CTD probe: data not shown) and with intermediate turbidity levels (water filtrations performed onboard gave values of suspended particulate matter concentrations ranging between 1 and 10 mg/L). Thus, water masses cannot be classified as extremely clear, knowing also that in the case of pure water the light is first absorbed in subsurface in the red wavelengths, then in the blue wavelengths at deeper levels, which leads to a decrease of K_{PAR} with depth [26]. Here K_{PAR} appears to be constant with depth. This can be first explained by a certain level of turbidity, and also by the fact that the turbidity appeared to be mainly induced by non-living material (water filtrations performed onboard gave values of chla concentrations ranging between 0.2 and 0.4 mg/m^3). Also in these winter conditions (mean wind intensity recorded onboard gave a value of 12 m/s with peaks up to 23 m/s, and a wave mean significant height of about 4 m) the water profile appeared well mixed with a bottom nepheloid layer corresponding to sediment resuspension (data not shown).

B. Glider versus satellites

Regarding possible matchups with L2 satellite products, unfortunately images from both MODIS and OLCI sensors could not be exploited because the high cloud cover happening during the five days of the sea survey prevented from any collocated comparison. Only VIIRS L2 products could be exploited during two days of the survey. Results obtained are presented hereafter. Regarding matchups with L4 cloud-free products, they are presented in the following.

1) L2 products from VIIRS: Matchups between the VIIRS sensor L2 product K_{PAR} data and the glider K_{PAR} data were reached on February 16 and 18, 2021 (Figure 5). Results obtained with the corrected algorithm of equation (6) showed that the L2 product K_{PAR} data range from 0.149 to 0.240 m^{-1}, with an average of 0.184 ± 0.032 m^{-1} (Figure 6); while K_{PAR} values with the former algorithm of equation (5) ranged from 0.18 to 0.3 m^{-1}, with an average of 0.22 ± 0.03 m^{-1}. Thus, when using the updated formula, L2 corrected products give for K_{PAR} a closer mean of values as the one issued from the glider, which measures a K_{PAR} average of 0.122 ± 0.007 m^{-1}. As a consequence, the resulting relative error found is 54%, compared to 93% with the previous algorithm.

Despite the significant proportion of missing data due to the presence of the thick cloud cover, L2 products are the most interesting: in fact, they correspond to the derived geophysical variables, at the same resolution as the level 1 (L1) satellite data. They correspond to a single L1 image where only atmospheric corrections and algorithms have been applied. Therefore, they have not undergone much processing and have not been averaged or interpolated (unlike the following L4 satellite products).

2) L4 products from MODIS, Optimal Interpolation (OI): Matchups obtained with the L4 products based on OI, and using the corrected algorithm of equation (6) are presented from Fig.7 to 11. They show a better agreement with the glider data compared to results obtained with the previous algorithm of equation (5). K_{PAR} values ranged from 0.153 to 0.212 m^{-1}, with an average of 0.18 ± 0.02 m^{-1} (Fig.12) while K_{PAR} values using the previous algorithm of equation (5) were between 0.20 and 0.26 m^{-1}, with an average of 0.23 ± 0.02 m^{-1}. The L4 product data obtained by OI also give a closer mean of values with the glider, whose average is 0.122 ± 0.007 m^{-1}, when the corrected algorithm is applied. The relative error between datasets is 49% compared to 86% with the previous algorithm.

Such average relative errors of 86% or 93% obtained with the previous algorithm of equation (5) for L2 VIIRS and L4 MODIS OI products, indicated that the Secchi depth (a metric estimate of the water transparency) would have shown values twice lower, and therefore would have been largely underestimated. It is significant in strategic areas, such as military submarine passage areas.

3) L4 products from MODIS, DINEOF Interpolation: Matchups results, presented from Fig.13 to 17, show K_{PAR} values between 0.081 and 0.111 m^{-1}, with an average of 0.1 ± 0.008 m^{-1} (Fig.18) while K_{PAR} values with the previous algorithm were between 0.12 and 0.14 m^{-1}, with an average of 0.13 ± 0.004 m^{-1}. Then the corrected algorithm gives K_{PAR} values slightly underestimated compared to the in situ glider data but still very close. The relative error shows a new average relative error of 18%, compared to 14% with the previous algorithm. The DINEOF method can be biased, like all interpolation methods, therefore this slight increase in relative error may be due to additional interpolation errors.

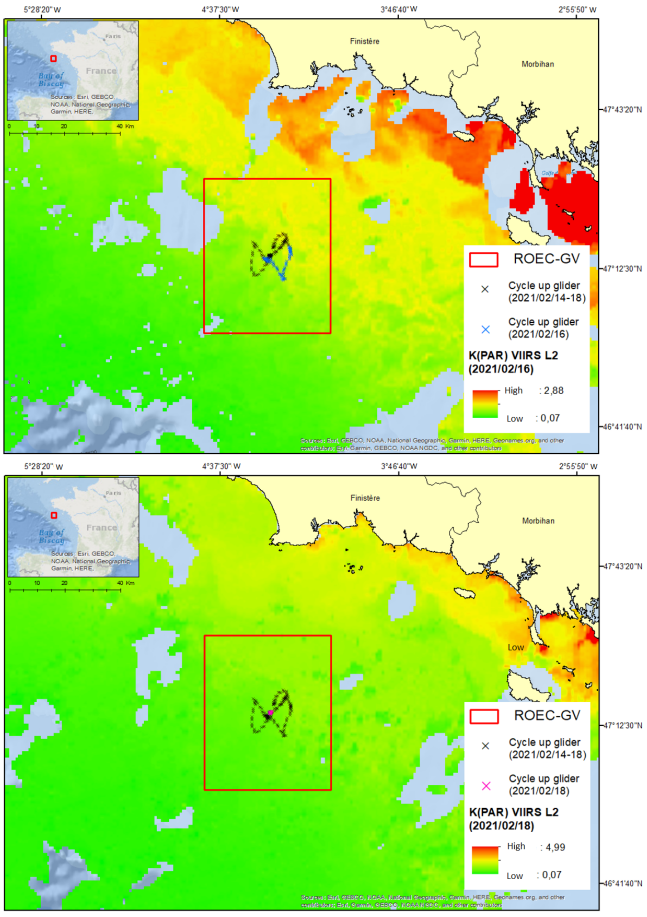

Fig. 5. Map of K_{PAR} (m^{-1}) VIIRS L2 data from February 16 (top, blue dots) and 18 (bottom, pink dots) 2021, in the glider deployment area. Black dots correspond to the total trajectory (cycles up only) performed by the glider during the whole campaign.

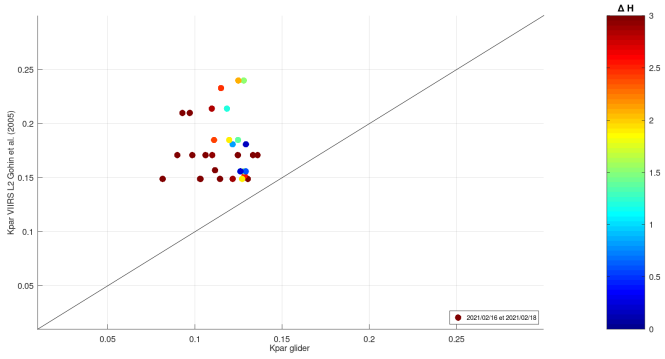

Fig. 6. Matchups between K_{PAR} (m^{-1}) data of L2 VIIRS products and K_{PAR} (m^{-1}) data of glider, for the February 16th and 18th. Brown points correspond to data where the acquisition exceeds the window of $\pm$ 3 hours (data not considered in the computed relative error).

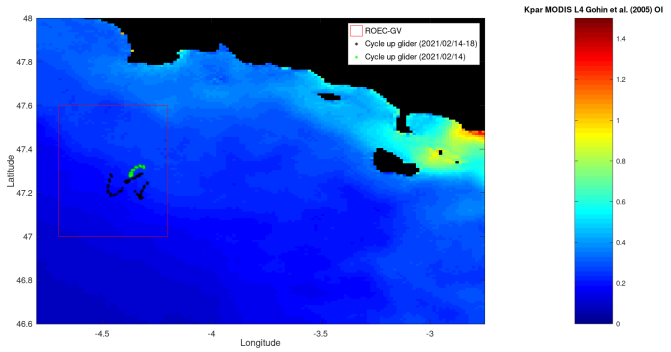

Fig. 7. Map of K_{PAR} (m^{-1}) data from L4 products (with OI), in the glider deployment area. Bright dots correspond to glider cycles up on 02/14/21 and black dots correspond to the total cycles up performed by the glider during the whole campaign

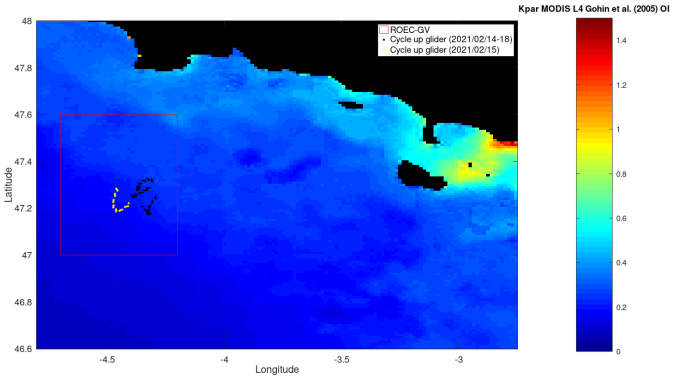

Fig. 8. Same as fig. 7 except for day 02/15/2021

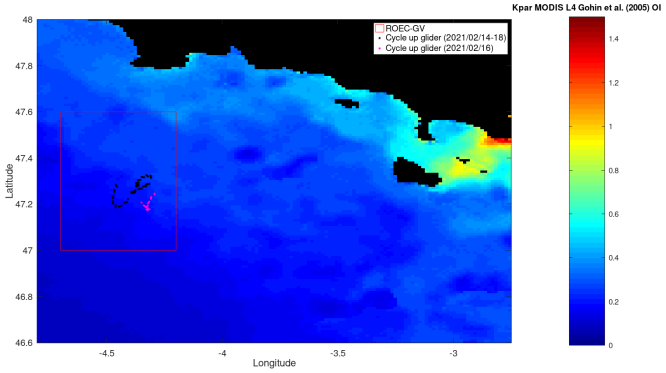

Fig. 9. Same as fig. 7 except for day 02/16/2021

In fact, by construction, the DINEOF interpolation smooths field data while removing short spatial wavelengths, as they preserve the first eigenvectors which, in practice, keep the longest spatial wavelengths. As a result, it also removes and smooths a certain variability that may exist at short spatial scales and thus induces lower K_{PAR} values. However, despite the increase of 4% in relative error, compared to the average relative error obtained with the previous algorithm, K_{PAR} values remain acceptable.

Moreover, in the Fig.12, a greater variability of K_{PAR} was

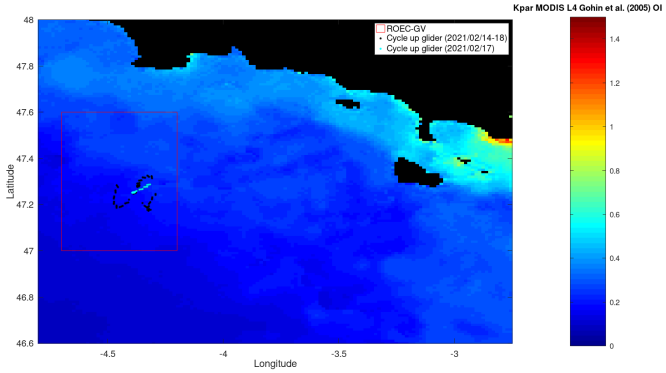

Fig. 10. Same as fig. 7 except for day 02/17/2021

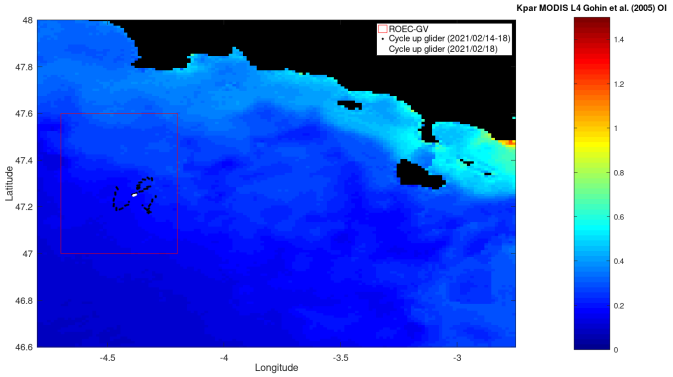

Fig. 11. Same as fig. 7 except for day 02/18/2021

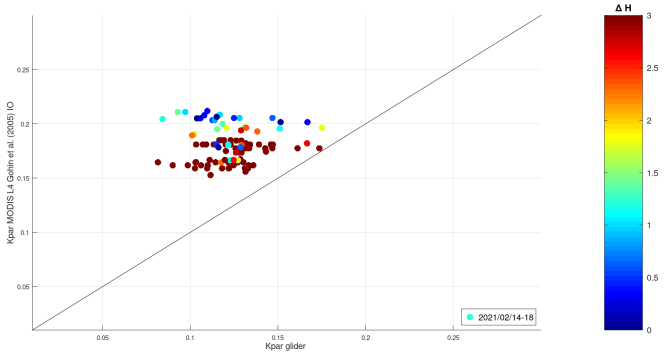

Fig. 12. Matchups between K_{PAR} (m^{-1}) data from L4 products (with OI) and those from the glider, for the five days of the campaign. Brown points correspond to data where the acquisition exceeds the window of $\pm$ 3 hours (data not considered in the computed relative error).

observed in glider data than in satellite data. This can come from two different processes. First, the spatial resolution of measurements issued from the glider is finer (with typically a horizontal distance of around 300 m between two yos) than the size of one ground satellite image pixel (around 1 km). So the glider is able to see finer spatial scales that satellite, and then it can possibly see the additional associated variability (not seen by the satellite). Secondly, the glider records all its parameters every second and can then observe the tidal high temporal frequency balance, that is able to affect the turbidity

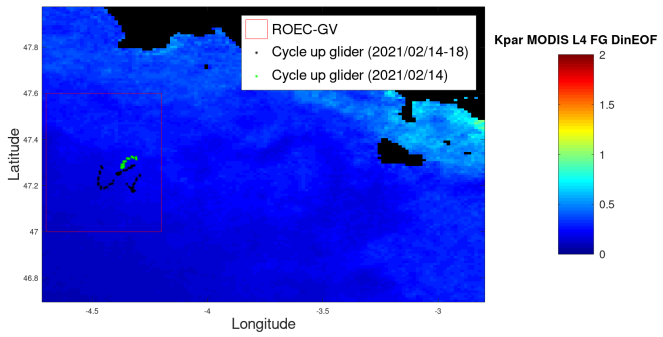

Fig. 13. Map of K_{PAR} (m^{-1}) data from L4 products (with DINEOF Interpolation) in the glider deployment area. Bright dots correspond to glider cycles up on 02/14/2021 and black dots correspond to the total cycles up performed by the glider during the whole campaign.

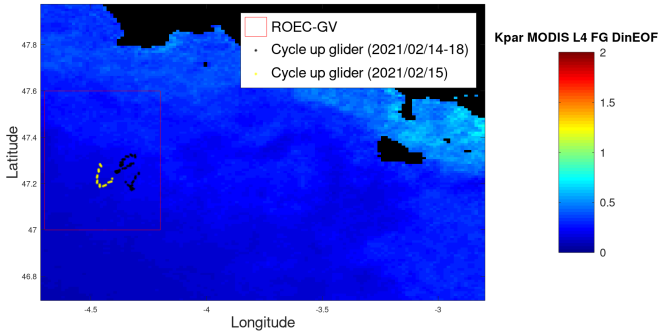

Fig. 14. Same as fig. 13 except for day 02/15/2021

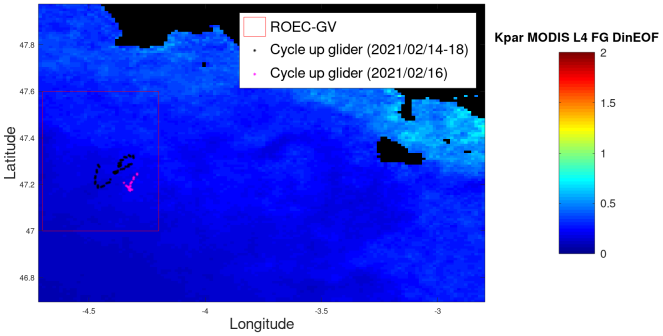

Fig. 15. Same as fig. 13 except for day 02/16/2021

signal as well, while the satellite only acquire one image per day. In consequence, the variability of this tidal signal can appear in practice as soon as the absolute value of ΔH is superior to 1 hour.

C. Empirical versus semi-analytical algorithms

The empirical algorithm [10] is widely used in scientific studies, particularly for Chla and NAP. The study [27] aimed to evaluate the overall performance of spatial and in situ monitoring to observe the dynamics of Chla, turbidity (NAP), and TSM (Total Suspended Matter) throughout the year 2017 in different coastal waters, including in the Bay of Biscay. Results confirmed a good overall agreement between satellite-derived

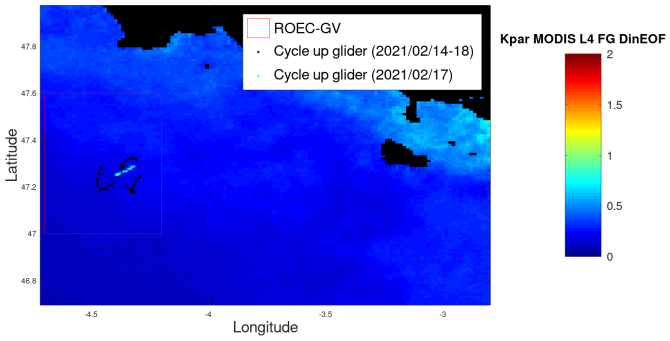

Fig. 16. Same as fig. 13 except for day 02/17/2021

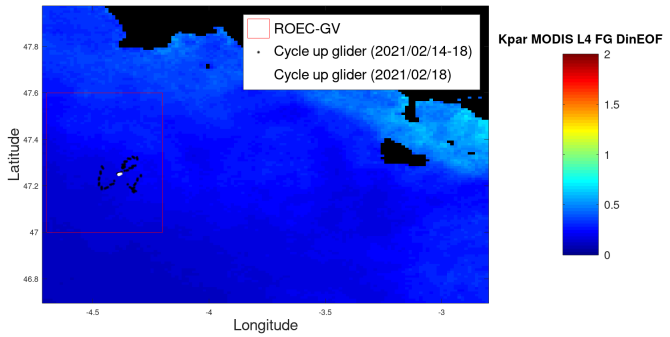

Fig. 17. Same as fig. 13 except for day 02/18/2021

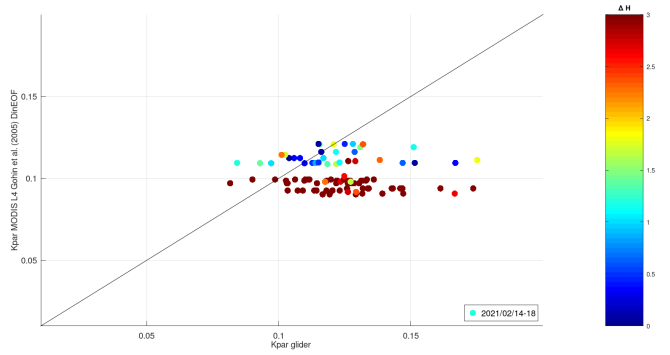

Fig. 18. Matchups between K_{PAR} (m^{-1}) data of L4 products (with DINEOF Interpolation) and K_{PAR} (m^{-1}) data of glider, for the five days of the campaign. Brown points correspond to data where the acquisition exceeds the window of $\pm$ 3 hours (data not considered in the computed relative error).

Chla observations and in situ observations. Same results are observed for turbidity (NAP): a good overall agreement was observed between the satellite and in situ time series of TSM and turbidity. So this empirical algorithm proved to be robust enough in recovering Chla and NAP concentrations over a wide range of water types. This empirical algorithm [10] is accurate because it is calibrated directly for the studied areas, unlike semi-analytical algorithms. Moreover, it seems adapted to waters with significant turbidity. Nevertheless, the associated formula (4) to compute K_{PAR} from the recovered Chla and NAP values appears to be unsuitable for clear waters. According to the study by [24], simple empirical techniques, such as empirical algorithms, have limited applicability due to inaccuracies when waters studied are clear. Furthermore, this algorithm does not take into account K_{PAR} values below 0.06 m^{-1}, while lower values exist when the water has the lowest turbidity values. Semi-analytical models, similar to the algorithm developed by the PML are based on the spectral signature of the main bio-physical components, in terms of absorption and scattering in water, including those of pure water. Therefore, semi-analytical algorithms could be more accurate when applied to reflectances in extremely clear waters. Unfortunately, the MELANGE campaign was unable to obtain matchups between the in situ glider data and the daily L3 OLCI product data generated by the PML algorithm. It would be relevant and interesting to reprocess the L2 MODIS product database with a semi-analytical algorithm, like the PML's one, which could be more suitable for clear waters, and which represents an important issue for the Navy, especially in submarine visual detection threshold.

IV. Conclusion

With irradiance sensors onboard, ocean gliders can measure light diffuse attenuation coefficients when they dive up or down and perform light attenuation sensing with depth, provided that the cloud cover does not vary (with a bias) during each dive. Doing so, they have an advantage in comparison with research vessels deploying irradiance sensors on CTD probe, which can be affected by the hull shadow (or their surface irradiance sensors affected by the mast shadow). This study allowed a comparison of K_{PAR} values obtained with a glider, a research vessel, and acquired by different satellite sensors, over the continental shelf of the Bay of Biscay, during a winter period. Both glider and ship measurements appeared to be consistent, while a satellite L2 product based on the VIIRS sensor gave different values. This discrepancy appeared to be caused by the empirical algorithm used to process K_{PAR} satellite values. A correction of this algorithm, to adapt it to clear waters (that were observed in the area) has been proposed and greatly improved the results. Matchups with L4 satellite products based on MODIS sensor acquisitions gave obviously more data for comparison but did not allow definitive conclusions due to the inherent errors from the two different interpolations applied (OI and DINEOF, that made these L4 products). A complementary study using a semi-analytical algorithm would be interesting to realize, because these algorithms may be more suitable for estimating K_{PAR} in clear waters. Also, further studies could involve spectral diffuse attenuation comparisons as well, because the SEAEXPLORER glider was able to measure not only K_{PAR} but also $K_{\mathrm{d}}380$, $K_{\mathrm{d}}490$ and $K_{\mathrm{d}}532$ as well during this campaign of the MELANGE project.

Acknowledgment

This research was funded by the French DGA (Direction Générale de l'Armement), through the MELANGE project. It was also supported by the French Space Agency CNES (Cen-

tre National d'Etudes Spatiales), through the ML4SECCHI project (Machine Learning for Secchi visibility).

REFERENCES

[1] Bourrin F. (CEFREM), Beguery L. (ALSEAMAR-ALCEN), Poisot F. (CENTRAL WEB), Jourdin F. (SHOM) (2019) Mesure en tEmps-réel des fLux sédimentAires en zoNe côtière à l'aide de GlidErs, response to tender for French ASTRID MATURATION projects, with the French "Agence Nationale de la Recherche" (ANR), ANR-14-ASTR-0021-01.

[2] Mengual, B. (2016) Variabilité spatio-temporelle des flux sédimentaires dans le Golfe de Gascogne: contributions relatives des forçages climatiques et des activités de chalutage (Doctoral dissertation, Brest).

[3] Claustre, H., Beguery, L., Pla, P. (2014) SEAEXPLORER glider breaks two world records. Sea Technol, 55(2014), 19-21.

[4] Kheireddine, M. (2014) Caractéristiques et origines de la variabilité diurne des propriétés optiques (Dissertation doctorale, Université Pierre et Marie Curie).

[5] Gratton, Y. (2002) Le krigeage: la méthode optimale d'interpolation spatiale. Les articles de l'Institut d'Analyse Géographique, 1(4).

[6] Saulquin, B., Gohin, F., Fanton d'Andon, O. (2019) Interpolated fields of satellite derived multi-algorithm chlorophyll-a estimates at global and European scales in the frame of the European Copernicus-Marine Environment Monitoring Service. Journal of Operational Oceanography, 12(1), 47-57.

[7] Alvera-Azcárate, A., Barth, A., Sirjacobs, D., Beckers, J. M. (2009) Enhancing temporal correlations in EOF expansions for the reconstruction of missing data using DINEOF. Ocean Science, 5(4), 475-485.

[8] Viellefon, P (2022) Analyse d'images satellitaires pour la prévision de la visibilité sous-marine, Master thesis report, Institut Polytechnique UNILASALLE, Beauvais, France, and Institut Universitaire et Européen de la Mer, Plouzané, France, 65pp.

[9] Bailey, S. W., Werdell, P. J. (2006) A multi-sensor approach for the on-orbit validation of ocean color satellite data products. Remote Sensing of Environment, 102(1-2), 12-23.

[10] Gohin, F. et al. (2005) 'Satellite-derived parameters for biological modelling in coastal waters: Illustration over the eastern continental shelf of the Bay of Biscay', Remote Sensing of Environment, 95(1), 29–46.

[11] Gohin, F., Druon, J. N., Lampert, L. (2002) A five channel chlorophyll concentration algorithm applied to SeaWiFS data processed by SeaDAS in coastal waters. International journal of remote sensing, 23(8), 1639-1661.

[12] Bowers, D.G., and Mitchelson-Jacob E. G. (1996) Inherent optical properties of the Irish Sea determined from underwater irradiance measurements. Estuarine, Coastal and Shelf Science, 43,433-447.

[13] Lafosse, L (2020) Forecasting underwater sighting range using remote sensing and artificial intelligence, Master thesis report, SeaTech engineering school, Toulon, France, and IHEDN Institute and University of Science and Technology of Hanoi, VietNam.

[14] Mason, J. D., Cone, M. T., and Fry, E. S. (2016). Ultraviolet (250–550 nm) absorption spectrum of pure water. Applied optics, 55(25), 7163-7172.

[15] Lin, J., Lee, Z., Ondrusek, M., Liu, X. (2018) Hyperspectral absorption and backscattering coefficients of bulk water retrieved from a combination of remote-sensing reflectance and attenuation coefficient. Optics Express, 26(2), A157-A177.

[16] Gordon, H.R. (1989) Can the Lambert-Beer law be applied to the diffuse attenuation coefficient of ocean water? Limnol. Oceanogr. 34(8), 1389-1409.

[17] Morel, A., Maritorena, S. (2001) Bio-optical properties of oceanic waters: A reappraisal. J. Geophys. Res., 106(C4), 7163-7180.

[18] Organelli, E. et al (2017) Two databases derived from BGC-Argo float measurements for marine biogeochemical and bio-optical applications. Earth Syst. Sci. Data, 9, 861–880, doi: 10.5194/essd-9-861-2017.

[19] Laforge, L. (2018) Comparaison de l'enneigement en Islande des produits satellitaires MODIS-Terra et MODIS-Aqua avec le modèle MAR lors de la période de fonte estivale, Master thesis report, Li'ege University, Belgium, https://matheo.uliege.be/bitstream/2268.2/5559/5/LAFORGE_memoire.pdf

[20] Otrio, G., and Cerutti-Maori, G. (2015) Les instruments optiques d'observation de la Terre. ISTE Group.

[21] IFREMER (2021a) MODIS composite images of radiances, chlorophyll-a, chlorophyll-a-nasa, suspended matters, turbidity, kpar, calcite, flags, optical tickness and coccoliths [IFREMER Algorithms] (res:1km), Centre d'Exploitation et de Recherche SATellitaire (CERSAT) product MODIS-RAD-CHL-CHL_NASA-SPM-TURB-KPAR-CALC-FLAG-Tau_865-Tau_862-Tau_869, ftp://ftp.ifremer.fr/ifremer/cersat/products/gridded/ocean-color/atlantic/modis/

[22] IFREMER (2021b) VIIRS composite images of radiances, chlorophyll-a, chlorophyll-a-nasa, suspended matters, turbidity, kpar, flags, optical tickness and coccoliths [IFREMER Algorithms] (res:1km), Centre d'Exploitation et de Recherche SATellitaire (CERSAT) product VIIRS-RAD-CHL-CHL_NASA-SPM-TURB-KPAR-FLAG-Tau_865-Tau_862-Tau_869, ftp://ftp.ifremer.fr/ifremer/cersat/products/gridded/ocean-color/atlantic/viirs/

[23] PML (2022) Level-3 satellite observation data, Copernicus Marine Environment Monitoring Service (CMEMS) product OCEANCOLOUR_ATL_OPTICS_L3_NRT_OBSERVATIONS_009_034, https://resources.marine.copernicus.eu/product-download/OCEANCOLOUR_ATL_OPTICS_L3_NRT_OBSERVATIONS_009_034

[24] Smyth, T.J., Moore, G.F., Hirata, T. Aiken, J. (2006) PML Inherent Optical Property model. Semianalytical model for the derivation of ocean color inherent optical properties: description, implementation, and performance assessment. Applied Optics, 45(31), 8116-8131.

[25] IFREMER (2021c) Analysed Chlorophyll-a for the IBI-ROOS area and analysed inorganic suspended matters for the IBI-ROOS area, , Centre d'Exploitation et de Recherche SATellitaire (CERSAT) products EUR-L4-CHL-ATL-v01-fv01-OI and EUR-L4-SPIM-ATL-v01-fv01-OI, ftp://ftp.ifremer.fr/ifremer/cersat/products/gridded/ocean-color/atlantic

[26] Lee, Z., Shang, S., Du, K., Wei, J. (2018) Resolving the long-standing puzzles about the observed Secchi depth relationships. Limnology and Oceanography, 63(6), 2321-2336.

[27] Gohin, F., Bryère, P., Lefebvre, A., Sauriau, P. G., Savoye, N., Vantrepotte, V., ... and Rétho, M. (2020) Satellite and in situ monitoring of Chl-a, Turbidity, and Total Suspended Matter in coastal waters: experience of the year 2017 along the French Coasts. Journal of Marine Science and Engineering, 8(9), 665.